

Neutron-diffraction study of the commensurate-incommensurate phase transition of deuterium monolayers physisorbed on graphite

H. Freimuth and H. Wiechert

Institut für Physik, Johannes Gutenberg-Universität, D-6500 Mainz, Federal Republic of Germany

H. P. Schildberg and H. J. Lauter

Institut Laue-Langevin, F-38042 Grenoble CEDEX, France

(Received 2 January 1990)

Neutron-diffraction measurements have been performed to investigate in detail the commensurate-incommensurate (C-IC) phase transition of deuterium monolayers physisorbed on the basal planes of graphite. Several novel features have been observed. Above completion of the commensurate $(\sqrt{3} \times \sqrt{3})R30^\circ$ phase a continuous phase transition to a striped superheavy domain-wall phase (α phase) occurs at temperatures below 7.3 K and densities between 1.05 and 1.16 (densities ρ are given in units of the complete C $\sqrt{3}$ phase). With increasing density the system undergoes a first-order phase transition to the γ phase. This phase ($1.19 \leq \rho \leq 1.32$) can be described as a strongly density modulated phase, which is equivalent to a hexagonal IC phase with heavy domain walls. Due to its special modulation and rotational epitaxy, the γ phase locks into higher-order commensurate phases, a $(5\sqrt{3} \times 5\sqrt{3})$ phase (δ phase) and a (4×4) phase (ϵ phase). A detailed description of domain-wall lattice models is presented. At densities beyond $\rho = 1.33$ a uniformly compressed IC phase was found. At temperatures above ≈ 7 K a reentrant fluid phase (β phase) is squeezed in between the C and IC phases, which is interpreted to be a domain-wall fluid. It evolves continuously to an isotropic fluid at temperatures above 18 K. Due to this unique sequence of phases occurring in a relatively wide density range ($1 \leq \rho \leq 1.33$), D_2 on graphite can be regarded as a model system for the study of the C-IC phase transition. A phase diagram is proposed based on neutron-diffraction and specific-heat measurements. The results are compared to those of H_2 /graphite and discussed in the light of current theories of the C-IC transition.

I. INTRODUCTION

Monolayers of physisorbed gases on solid surfaces can form two completely different types of solid phases: (a) Phases which are governed by the adsorbate-adsorbate interactions with only small lateral contributions from the substrate potential. In this case the lattice constants of the surface layer will generally be incommensurate (IC phase) with the substrate lattice periodicity. The rotational epitaxy of these phases can be described by the Novaco-McTague theory.¹ (b) Phases where the substrate-adsorbate interaction forces the adsorbed particles into substrate potential minima. The lattice constants of these structures are commensurate (C phase) with respect to the substrate lattice constants. These phases are described by lattice-gas models.² One of the most fascinating issues in the study of physisorbed monolayers is the transition between these two types of solids.³

The basic ideas of the commensurate-incommensurate (C-IC) transition were developed by Frank and Van der Merwe⁴ in a one-dimensional (1D) model. They found that the competition between adsorbate-substrate and adsorbate-adsorbate interactions can lead to the formation of misfit dislocations (1D domain walls) separating commensurate regions. In two dimensions the problem becomes more complicated. Bak *et al.*⁵ showed that the domain walls can be arranged either parallel to each other

or in a hexagonal pattern depending on the domain-wall crossing energy. In case of a striped array of domain-walls the C-IC transition is continuous, whereas in case of a hexagonal array it is discontinuous. Villain⁶ noted that a deformation of the hexagonal network costs no energy and therefore, due to the contribution of the entropy to the free energy, the hexagonal pattern is favored. The C-IC transition is still first order with a narrow hexagonal domain-wall phase squeezed in between the commensurate and striped phases. At nonzero temperature contributions of wall fluctuations become relevant as was first pointed out by Pokrovsky and Talapov⁷ for a striped array of parallel domain walls. They lead to domain-wall meandering and effective repulsions between the walls due to wall collisions, which make the C-IC transition to the striped phase continuous. For low IC densities (large distances between the domain walls) or high temperatures the elastic constants associated with the wall fluctuations need not be high enough to stabilize this phase against spontaneous creation of free dislocations as Coppersmith *et al.*⁸ have predicted. Thus, the weak IC phase may be a reentrant fluid (domain-wall fluid) which can extend down to $T=0$ K. Kardar and Berker⁹ found out that the degeneracy of the three equivalent sublattices present in the commensurate phase leads to two types of domain walls (heavy and superheavy) with different energies. This introduced a cer-

tain helicity (or chirality) into the problem described by a helical Potts model. An application of this model to the case of krypton adsorbed on graphite^{10,11} has been very successful in producing a phase diagram in close resemblance to that observed experimentally.¹²

Most of the theoretical work had been done on the heavy rare gases until 1985 when Halpin-Healy and Kardar¹³ used a striped helical Potts model to calculate the complete phase diagram of the first layer of helium adsorbed on graphite. The C-IC transition of this model proved to be rather complicated with a sequence of C phase, a domain-wall fluid, a striped domain-wall phase, a coexistence of striped and hexagonal phases, and a hexagonal domain-wall phase.

Recently, the C-IC transition has been studied experimentally in a number of systems, e.g., Kr/graphite,¹² Xe/Pt,¹⁴ and bromine-intercalated graphite,¹⁵ and various domain-wall phases could be detected. Related phenomena are, e.g., the occurrence of charge-density waves in layered metal chalcogenides¹⁶ and of modulated magnetic structures in rare-earth compounds.¹⁷

In this paper we present our results on the hydrogen isotopes H₂ and D₂ adsorbed on graphite. The phase diagram at the C-IC transition of H₂/graphite¹⁸⁻²¹ is similar to the phase diagrams of the He isotopes physisorbed on graphite,^{22,23} whereas D₂ exhibits a much more detailed behavior.^{21,24,25} The C-IC transition of D₂ is spread out over a larger coverage range than in any other system and can therefore be studied in great detail. By this fact deuterium monolayers on graphite can be regarded as a model system for the C-IC transition.

Up until 1984 nothing else was known of the hydrogen isotopes physisorbed on graphite but that both H₂ and D₂ form a commensurate ($\sqrt{3} \times \sqrt{3}$)R30° structure and at higher coverages an equilateral triangular incommensurate structure.²⁶⁻²⁸ Recently details of the phase diagrams were obtained by specific-heat measurements^{18-21,24,25,29-31} and revealed important new phenomena at the C-IC transition of both systems.^{18-21,24,25}

Figure 1 shows the phase diagrams obtained by specific-heat measurements of H₂ and D₂ physisorbed on graphite in the C-IC transition region.^{18,19,21,24,25,31} The density ρ is given in units of the ideal commensurate $\sqrt{3}$ phase, i.e., all adsorption sites of the phase are occupied. H₂/graphite exhibits a single solid phase (α phase) between the C and the IC phases [see Fig. 1(b)], which has been interpreted as a striped domain-wall phase with superheavy walls^{21,31} and a reentrant fluid (β phase). For D₂/graphite four intermediate low-temperature phases ($\alpha, \gamma, \delta, \epsilon$) have been distinguished by specific-heat measurements^{21,24,25} [see Fig. 1(a)]. At $\rho > 1$ and low temperatures the C phase is followed by the α phase, the γ phase, the ϵ phase, and the IC phase. Inside the coverage and temperature range of the γ phase a small isolated region (δ phase) could be detected. Contrary to H₂/graphite, where a reentrant melting between the α phase and the IC phase is observed at least down to 5 K, the β phase of D₂/graphite is confined to higher temperatures. Between the β phase and the isotropic fluid a broad transition region is indicated by flat specific-heat anomalies near 20 K.

The behavior of H₂/graphite has been described previously³¹ and will be compared in this paper to the far more complicated behavior of D₂/graphite. Some neutron-diffraction results of D₂ monolayers were previously published in Refs. 21, 25, 32-35, and in Ref. 36 in combination with low-energy electron-diffraction (LEED) results. The present paper gives a more detailed account of the neutron-diffraction data. The main aim is to clarify the nature of the different intermediate phases first observed in the specific-heat experiments.^{21,24,25} The results presented are complementary to those obtained by LEED by Cui and Fain.^{36,37} The advantage compared to LEED is that neutron-diffraction spectra do not suffer from multiple-scattering effects, so that an analysis of peak intensities for exact structure determinations can be performed. On the other hand, in LEED measurements graphite single crystals can be used and therefore additional information on the orientational epitaxy of the in-

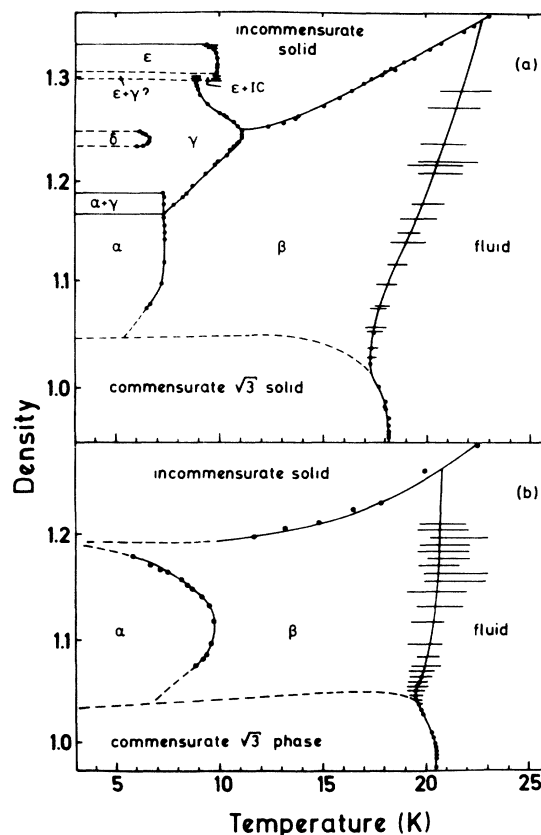


FIG. 1. Proposed phase diagrams for (a) D₂ and (b) H₂ adsorbed on graphite in the commensurate-incommensurate transition region. The points indicate the positions of heat-capacity anomalies from Refs. 18, 19, 21, 24, 25, and 31. The larger error bars at the transition line between the β and the fluid phases are due to the uncertainty in determining the locations of very broad specific-heat maxima. The solid lines are phase boundaries inferred from experimental data. The dashed lines are speculative phase boundaries. The phase diagrams show several intermediate phases ($\alpha, \beta, \gamma, \delta$, and ϵ phases) between the C and IC phases.

intermediate phases can be deduced. Thus, a combination of the results of both methods is crucial to get a comprehensive understanding of the nature of the intermediate phases.

The remainder of this paper is organized as follows. In Sec. II experimental details are described. Diffraction spectra of all phases are presented in Sec. III. The structure of the α phase is discussed in Sec. IV. Section V describes the γ phase and Sec. VI the δ and ϵ phases. The relations to theory and other experimental work is discussed in Sec. VII. The paper closes with a short summary of the main features of the C-IC transition of D_2 /graphite in Sec. VIII.

II. EXPERIMENTAL DETAILS

Most of the neutron-diffraction measurements presented in this paper were performed on the two-axes powder diffractometer D1B with a wavelength of $\lambda=2.52$ Å at the Institut Laue-Langevin (ILL) in Grenoble. This instrument uses a multidetector with 400 active cells covering an angular range of $2\theta=80^\circ$. The detector allowed a simultaneous recording of scattered neutrons from 1.05 to 3.92 Å⁻¹. The counting times were up to 4 h per spectrum. The instrumental resolution in θ varies from $\approx 0.2^\circ$ (FWHM, $\Delta Q \approx 0.016$ Å⁻¹) at the position of the commensurate $\sqrt{3}$ peak to $\approx 0.45^\circ$ (FWHM, $\Delta Q \approx 0.028$ Å⁻¹) at the position of the higher-order peaks. The sample consisted of a stack of exfoliated Papyex (trademark of Carbon Lorraine) graphite sheets closely packed into a cylindrical aluminum cell and oriented parallel to the scattering plane. To discriminate the scattering of the graphite substrate and the aluminum cell, a spectrum with zero filling was taken and was subtracted as background from the data.

In addition, measurements were performed with a high-quality ZYX graphite sample (trademark of Union Carbide) on the two-axes diffractometer D16 at the ILL with a wavelength of 4.52 Å. The ZYX sample has larger single crystallite surfaces (mean diameter ≈ 2000 Å) than Papyex (≈ 250 Å).

The gas was introduced into the sample cell at 20 K, annealed at 40 K, and then slowly cooled down. We used natural D_2 gas, 99.7% pure, containing 33% para- D_2 molecules at room temperature. Because of the uncertainty in the conversion rate given in the literature,^{38,39} we are not sure whether the portion of para- D_2 molecules was totally negligible during the measurements. Nevertheless, we assume a free-rotator behavior and no orientational ordering effects on the observed phases.

The coverage calibration was achieved in two ways: (a) We measured a number of coverages near the complete commensurate $\sqrt{3}$ layer and defined the amount of adsorbed D_2 which yielded the most intense Bragg reflection at $T=2$ K as $\rho=1$. This coverage scale was in good agreement with that of Ref. 24 obtained by observing the largest specific-heat disordering anomaly. (b) The number of particles per unit area was calculated from the position of a Bragg reflection of the equilateral triangular IC phase by assuming a homogeneous structure of the adsorbate on the whole graphite surface. This resulted in a

density scale which is in good agreement with LEED data.^{36,37} We found that the density scale determined by method (b) yielded 4% lower values than the coverage scale (a). The same effect had been observed for H_2 /graphite where the difference between coverage and density scale was about 2%.³¹ The reason for the difference between both methods is not totally clear, but the offset may be caused by surface defects and interstitials. To avoid confusion in this paper we refer only to the density scale determined by method (b) as the scale given directly by the incommensurate structure of the adsorbate. In constructing the phase diagram (Fig. 1) the specific-heat coverages of Refs. 18, 19, 24, 25, and 31 were multiplied by 0.96 for D_2 and 0.98 for H_2 to agree with this density scale.

In order to compare measured with calculated neutron-diffraction-peak intensities at the positions of Bragg reflections, we used the following expression:^{40,41}

$$I(hk) \sim \frac{m_{hk} |F_{hk}|^2 f^2(\theta_{hk}) e^{-2W}}{(\sin\theta_{hk})^{3/2}}. \quad (1)$$

Here m_{hk} represents the multiplicity of the hk -th reflection, F_{hk} is the structure factor of the 2D lattice, θ_{hk} is the scattering angle at the position of the Bragg reflection, $f(\theta_{hk})$ is the molecular form factor, e^{-2W} identifies the Debye-Waller factor, and $(\sin\theta_{hk})^{3/2}$ the Lorentzian factor. We assume that molecular orientational order does not occur in the temperature region of our investigation.³⁸ In this circumstance and for small- Q values the molecular form factor is given by⁴²

$$f(\theta) = 2j_0(\frac{1}{2}Ql), \quad (2)$$

where j_0 is the zeroth-order spherical Bessel function, $|Q| = (4\pi/\lambda)\sin\theta$, and l is the bond length in the molecule (0.742 Å for D_2). In the Q range of our scans $f(\theta)$ decreases monotonically with increasing scattering angle.

The analysis of the experimental data was performed by fitting powder-averaged Lorentzian-squared intrinsic line shapes to the data.⁴³ Empirically we found that these line shapes gave the best fits to our relatively low-resolution neutron-diffraction measurements. This type of intrinsic line shape of the incommensurate phase may be caused by pinning of dislocations to steps or imperfections as observed for spin systems in random magnetic fields.^{44,45} The Lorentzian-squared line shape can be regarded as a reasonable approximation of the power-law structure factor in the modified form of Dutta and Sinha.⁴⁶ Within the low resolution of our experiment we could not see any line-shape changes in the different phases observed. Another reason might be due to the fact that exfoliated graphite samples have a relatively broad distribution of crystallite sizes, which might obscure intrinsic line-shape effects as was argued in Ref. 43. In the calculations we used a mosaic spread of 30° FWHM of the surface basal planes and an isotropic powder percentage of 70% for the Papyex sample,⁴⁷ which gave the best fit to the highest diffraction peak of the $\sqrt{3}$ phase. In the case of the ZYX-graphite sample, the fit parameters were 40% for the isotropic powder portion and 22° FWHM for the mosaic spread.

III. RESULTS

A complete spectrum of D_2 /graphite at the density $\rho=1.34$ and temperature $T=4$ K is presented in Fig. 2. Two peaks of the IC structure can be clearly observed, the main peak (10) at $Q=1.97 \text{ \AA}^{-1}$ and a higher-order peak (11) at $Q=3.41 \text{ \AA}^{-1}$. The gap in the spectrum near 3.0 \AA^{-1} and the enhanced scattering near 1.88 \AA^{-1} are due to imperfect subtraction of background reflections because of interference with the graphite substrate.

From the drop of the intensity from the (10) to the (11) reflection an estimate of the Debye-Waller factor could be obtained in a similar way as done in Ref. 41 for Ar monolayers. Hereby we applied the relation (1) with

$$\exp(-2W) = \exp[-0.5(Q^2 \langle u^2 \rangle)]$$

and corrected the measured peak intensities by the molecular form factor and the Lorentzian factor. The mean-square displacement for the D_2 molecules in the IC phase was found to be $\langle u^2 \rangle = 0.25 \text{ \AA}^2$. Within experimental error the same value was obtained for the commensurate phase from the (10) and (20) reflections. [The (11) reflection of the C phase coincides with the (100) reflection of the graphite substrate and cannot be observed.] From inelastic measurements in the C phase, recently a value of $\langle u^2 \rangle = 0.21 \text{ \AA}^2$ has been inferred⁴⁸ consistent with the present result. For comparison, Ni and Bruch⁴⁹ using a Lennard-Jones model for the intermolecular potential calculated with the Hartree and Jastrow perturbation approximations values of $\langle u^2 \rangle = 0.26 \text{ \AA}^2$ and $\langle u^2 \rangle = 0.66 \text{ \AA}^2$, respectively, and Novaco and Wroblewski^{50,51} applying self-consistent phonon theory deduced $\langle u^2 \rangle = 0.27 \text{ \AA}^2$ parallel to the surface for the C phase. In calculations based on the Silvera-Goldmann

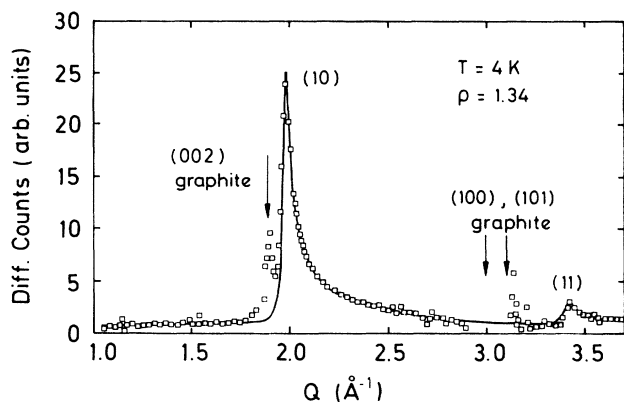


FIG. 2. Neutron-diffraction spectrum from D_2 adsorbed on graphite (Papyex) showing the (10) and (11) Bragg peaks of the IC equilateral triangular structure at $\rho=1.34$ and $T=4$ K. The background of the empty cell has been subtracted from the data. The arrows indicate the locations of the (002), (100), and (101) graphite substrate reflections, where some residual scattering remains because of imperfect subtraction of the background due to interference with the substrate structure. The solid line represents a fit of a powder-averaged Lorentzian-squared line shape with a coherence length of 250 \AA to the data.

potential model Gottlieb and Bruch^{52,53} obtained values for the mean-square lateral displacement for the C phase between 0.285 and 0.328 \AA^2 depending on the potential parameters applied. These authors also showed⁵³ that the results depend strongly on the value adopted for the corrugation amplitude in the holding potential. If the corrugation amplitude is included in the Jastrow function, the high values for $\langle u^2 \rangle$ of Ref. 49 are reduced and become closer to the Hartree estimates. Thus, one may conclude that there is fair agreement between theory and experiment.

Figure 3 shows spectra at six different densities at low temperatures throughout the C-IC transition region. No reliable data could be taken near the (002) graphite reflection at $Q=1.876 \text{ \AA}^{-1}$. Data points in this region are omitted in the figures except for $\rho=1.24$, where, by accident, the interference with the graphite is hardly seen

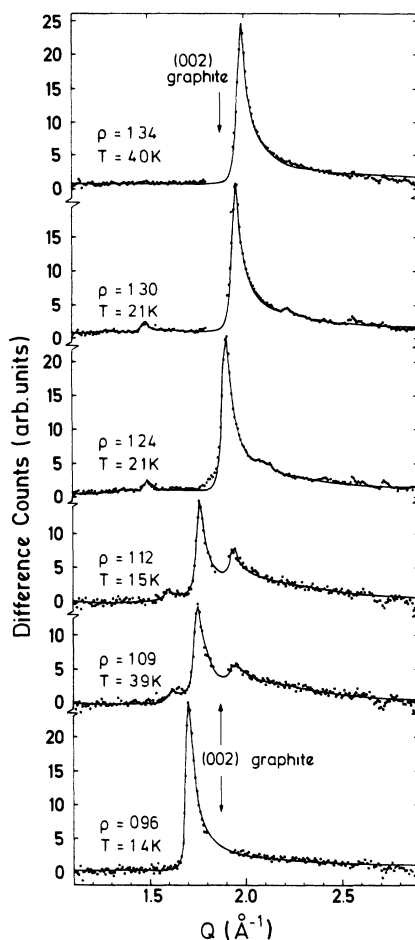


FIG. 3. Evolution of diffraction profiles from the commensurate to the incommensurate phase at low temperatures. The spectra taken in the α phase ($\rho=1.09$ and 1.12) and in the γ phase ($\rho=1.24$ and 1.30) clearly show the occurrence of satellite reflections in addition to the main reflection. The arrows indicate the position of the disturbing (002)-graphite peak, where data mostly have been omitted for clarity. The solid lines are fits of powder-averaged Lorentzian-squared line shapes to the data.

and an estimate can be made of the main peak position of $Q=1.89 \text{ \AA}^{-1}$.

In order to outline the general behavior of the Bragg reflections, Fig. 4 gives a survey of all peak positions obtained at the lowest investigated temperatures with $Q < 2.5 \text{ \AA}^{-1}$ versus the square root of the density. The peaks are labeled by numbers (for details see Secs. IV and V). The density regions of the different phases are indicated by dashed vertical lines. The completion of the first monolayer is observed at $\sqrt{\rho} \approx 1.245$. This refers to a density of $\rho \approx 1.55$ (i.e., 0.0987 particles per \AA^2), somewhat higher than $\rho \approx 1.45$ (i.e., 0.0927 particles per \AA^2) for H_2 ,³¹ indicating that the equilateral triangular IC solid of D_2 can be closer packed than the H_2 solid analogous to the bulk systems.^{26,27} From the Q value at the complete monolayer density a nearest-neighbor distance of 3.42 \AA can be inferred for D_2 compared to 3.53 \AA found for H_2 .³¹ Both values are in good agreement with those given by Nielsen *et al.*^{26,27} The solid line at $\rho \leq 1$ indicates the commensurate position Q_C . Within the α and γ region the solid lines refer to calculated peak positions as explained in the text. Details will be given in Secs. IV and V. The long straight line connecting $\rho=1$ with monolayer completion at $\rho=1.55$ is calculated under the assumption that all molecules are accommodated in a homogeneous equilaterally spaced triangular lattice covering the total surface of graphite. Beyond monolayer completion the small slope of the line reflects the slight compression of the first layer by the formation of the second layer.

The spectrum at $\rho=0.96$ in Fig. 3 gives an example of a strong peak at the commensurate position $Q_C=1.703 \text{ \AA}^{-1}$. The coherence length of the structure is determined to $\approx 250 \text{ \AA}$, which is regarded as the mean crystallite size of the Papyex substrate. For all coverages $\rho < 1$ the Bragg reflection remains at Q_C (Fig. 4). An increase

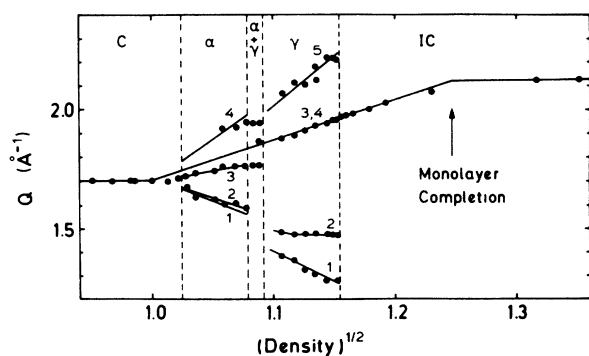


FIG. 4. The neutron-diffraction peak position Q vs the square root of density ρ for $\text{D}_2/\text{graphite}$ at $2 \leq T \leq 4 \text{ K}$. The observed peaks are labeled by numbers 1–5. The dashed vertical lines mark the density ranges of the different phases. Within the α and γ regions the solid lines refer to calculated peak positions as explained in the text. The long straight line between $\rho=1$ and monolayer completion at $\rho=1.55$ indicates the expected peak positions, if all molecules were incorporated in a homogeneous equilaterally spaced triangular IC structure. The transition between the α and the γ phases occurs via a coexistence range ($\alpha+\gamma$).

in coverage leads, after an overfilling of about 2% of the best C phase, to a shift of the main peak to higher Q values (Fig. 4). At densities $1.05 \leq \rho \leq 1.16$ the diffraction pattern of the α phase can be observed. Two examples are shown in Fig. 3 at $\rho=1.09$ and 1.12 . The low- Q satellite is far enough removed from the main peak to be clearly observed at both coverages. The high- Q satellite, although clearly visible, is strongly disturbed by the (002)-graphite reflection, so that its position cannot be determined accurately at $\rho=1.09$. This improves at higher coverages. The shift of the α -phase peaks comes to a halt at $\rho \approx 1.16$ (see Fig. 4). A further increase of the coverage results in a continuous decrease of the peak intensity. Simultaneously, at the position of the equilateral triangular IC structure, indicated by the straight line at $1.0 \leq \sqrt{\rho} \leq 1.25$ in Fig. 4, a new main peak appears. Unfortunately, the new peak is located near the (002)-graphite reflection and therefore cannot be observed until it reaches nearly its full height. In addition, satellites appear further away from the main peak than in the α phase indicating the γ phase. These observations clearly reveal that the α - γ transition proceeds via a coexistence region at $\rho \approx 1.16$ – 1.18 [see phase diagram, Fig. 1(a)]. Two examples of spectra of the γ phase at $\rho=1.24$ and 1.30 are shown in Fig. 3. At $\rho=1.24$ the main peak is found at $Q=1.89 \text{ \AA}^{-1}$ near the (002)-graphite reflection and shifts along the IC peak position (Fig. 4) to $Q=1.95 \text{ \AA}^{-1}$ at $\rho=1.30$. Two satellites can be clearly observed. The low- Q one nearly stays at constant position ($Q \approx 1.48 \text{ \AA}^{-1}$), whereas the high- Q one shifts with increasing coverage ($Q=2.09 \text{ \AA}^{-1}$ at $\rho=1.24$ and $Q=2.21 \text{ \AA}^{-1}$ at $\rho=1.30$). In addition, a very tiny anomaly was detected at smaller angles ($Q=1.36 \text{ \AA}^{-1}$ at $\rho=1.24$ and $Q=1.28 \text{ \AA}^{-1}$ at $\rho=1.30$). The anomaly has been observed in all spectra of the γ phase moving to lower Q with increasing coverage, and we therefore identify it with a third satellite (1). The two low- Q satellites (1) and (2) are shown on an enlarged scale in Fig. 5 at the coverages $\rho=1.26$ and

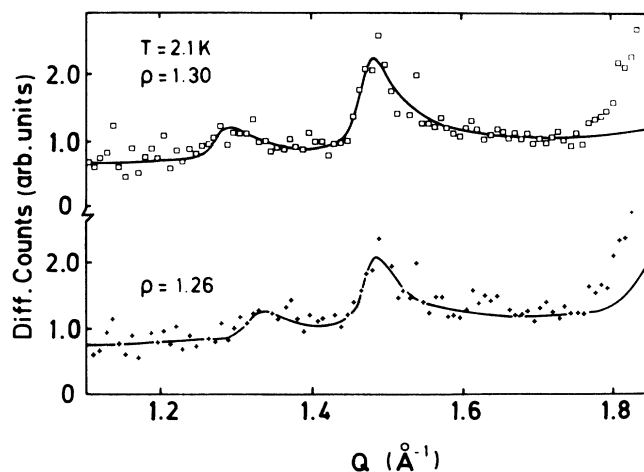


FIG. 5. A portion of the diffraction profiles in the low- Q range at two densities of the γ phase ($\rho=1.26$ and 1.3) and a temperature of 2.1 K magnified to prove the existence of a third satellite at low- Q values. The solid line represents the best fit of a Lorentzian-squared structure factor.

1.30. Although the intensity of the anomaly near $Q=1.30 \text{ \AA}^{-1}$ is very small, it can be clearly observed as it shifts from $Q=1.28 \text{ \AA}^{-1}$ at $\rho=1.30$ to $Q=1.32 \text{ \AA}^{-1}$ at $\rho=1.26$.

The increase of the coverage up to $\sqrt{\rho} \approx 1.15$ produces a continuous shift of all reflections of the γ phase (Fig. 4). Considering the peak position alone no signal of the δ and ϵ phases can be detected. At $\sqrt{\rho} \approx 1.15$ the satellites vanish (Fig. 4) and only the (10) and (11) peaks of the equilateral triangular IC phase (Figs. 2 and 3: $\rho=1.34$) remain. The IC structure can be compressed up to $\sqrt{\rho} \approx 1.245$ where the densest monolayer is reached.

In Figs. 6 and 8 the melting behavior of the intermediate phases is shown. Figure 6 demonstrates the melting of the α phase at $\rho=1.12$ via the β phase towards an isotropic fluid. At the temperatures $T=1.5, 3.9,$ and 6.9 K the typical diffraction spectrum of the α phase remains nearly unchanged. When the melting line of the α phase at $T \approx 7.3 \text{ K}$ is crossed, the triple-peak structure vanishes and a broad bump remains. The coherence length is still $\approx 20 \text{ \AA}^{-1}$ indicating that the β phase is a highly correlated liquid. The shape of the signal is hardly affected by an increase of temperature from 7.9 to 15.9 K , but becomes significantly flatter when raising the temperature above $T \approx 18 \text{ K}$, that means crossing the transition line between the β and the isotropic fluid phase.

On the melting of the α phase, a discontinuous jump of the main peak position was observed. Further temperature increase results in a peak shift indicating a compression of the β fluid. This is illustrated in Fig. 7, where the peak positions are plotted versus temperature. The data of D_2 at $\rho=1.119$ (solid circles) are compared with those

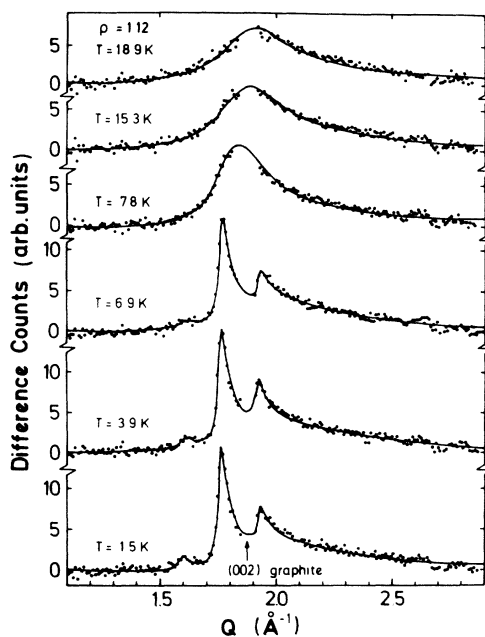


FIG. 6. Diffraction profiles showing the melting of the α phase to the β phase ($T \approx 7.3 \text{ K}$) and the transition of the β phase to the isotropic fluid phase ($T \approx 18 \text{ K}$) at $\rho=1.12$. The solid lines are best fits using a Lorentzian-squared line shape.

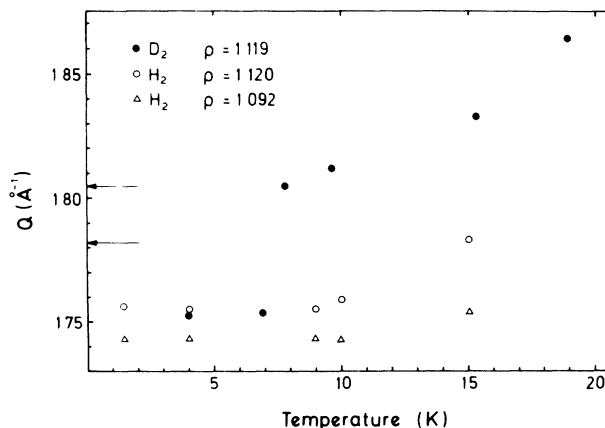


FIG. 7. The positions (Q) of diffraction peaks of D_2 /graphite (solid circles) as a function of temperature at $\rho=1.119$. The open circles ($\rho=1.120$) and open triangles ($\rho=1.092$) represent for comparison results of H_2 /graphite. The arrows show the calculated peak positions of an unmodulated equilateral triangular IC phase at densities $\rho=1.12$ and 1.092 .

of H_2 at $\rho=1.120$ (open circles) and $\rho=1.092$ (open triangles). Contrary to D_2 the melting of the α phase of H_2 at $T \approx 9.5 \text{ K}$ shows practically no peak shift at all, it seems to be continuous. Only in the β phase a slight compression occurs. The arrows indicate the calculated Q values of Bragg reflections of equilaterally spaced triangular IC structures at densities $\rho=1.120$ and 1.092 as explained in the discussion of Fig. 4. The figure clearly reveals that on the melting of the α phase of D_2 ($T \approx 7.3 \text{ K}$), the main peak position ($Q=1.753 \text{ \AA}^{-1}$) discontinuously jumps to the position of the IC phase ($Q=1.805 \text{ \AA}^{-1}$) at the same density.

Figure 8 displays spectra at $\rho=1.28$. Increasing the temperature from 2.1 to 18 K results in a sequence of γ phase, equilateral triangular IC phase, and β phase. At $T=2.1$ and 7.8 K the spectrum of the γ phase is observed, recognizable by the satellites. The satellites vanished at $T=10.4$ and 12.5 K . Only the (10) peak of the IC phase remains. At $T=18 \text{ K}$ the IC phase is melted into the β phase. No shift of the main peak at the γ -IC transition was observed. At the melting of the IC phase into the β phase a small compression of the fluid sets in, but no discontinuous jump of the peak position comparable to the peak shift at the α - β transition of D_2 monolayers did occur. The isotropic fluid at higher temperature $T > 20 \text{ K}$ is not shown in Fig. 8.

In order to check whether the results are influenced by the constraints of the Papyex substrate we have performed measurements on ZYX graphite. The crystallite sizes of ZYX are typically an order of magnitude larger than those of Papyex so that finite-size effects should be significantly diminished. In addition, the better orientation of the crystallites in ZYX reduces the influence of the (002) graphite reflection. Figure 9 displays two examples of ZYX spectra: the α phase at $\rho=1.13$ and the γ phase at $\rho=1.30$. Due to the larger crystallite sizes the coherence lengths of the peaks are larger than for the Papyex

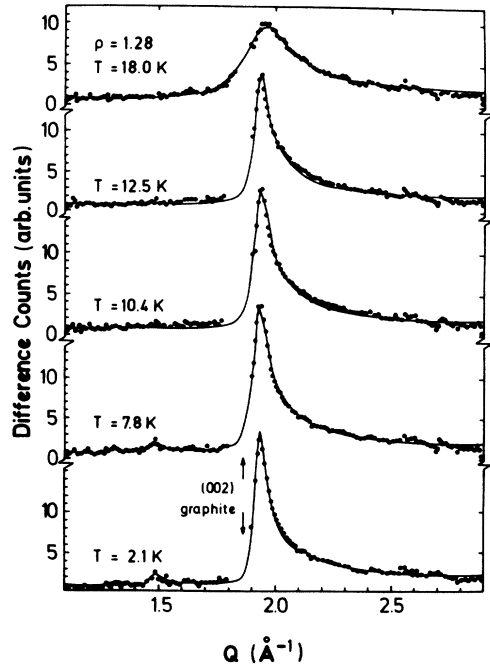


FIG. 8. Sequence of diffraction profiles showing the transition of the γ phase via the IC phase to the β phase at $\rho=1.28$. Lorentzian-squared line shapes are fitted to the data (solid lines).

spectra ($\geq 1000 \text{ \AA}^{-1}$). This effect and the higher resolution of the D16 spectrometer results in a better separation of the satellites from the main peak, especially in the α phase. Concerning the peak positions and the intensity ratios, the ZYX results are identical to the Papyex results.

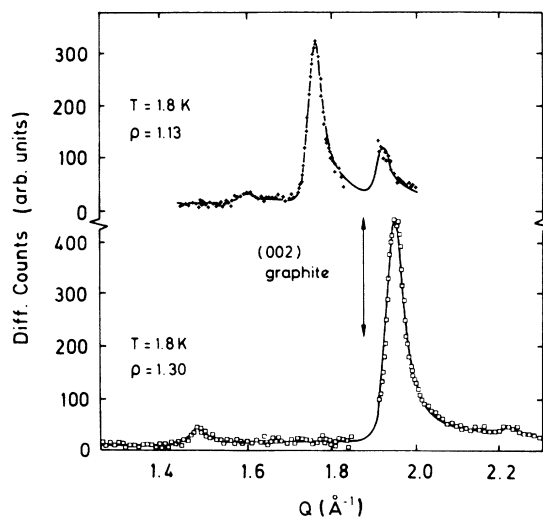


FIG. 9. Diffraction spectra of D_2 adsorbed on ZYX graphite in the α phase at $\rho=1.13$ (upper panel) and in the γ phase at $\rho=1.30$ (lower panel) and $T=1.8 \text{ K}$. The solid lines are best fits using a Lorentzian-squared structure factor with a coherence length of 1000 \AA . The arrow indicates the range of disturbing overlap with the graphite (002) reflection.

Details of the ZYX results are planned to be published elsewhere.

IV. THE α PHASE

In order to explain the observed diffraction peaks of the α phase and their density dependence within modern concepts of the theory of the C-IC transition,^{3-11,13} we considered the α phase as a striped domain-wall phase with superheavy walls of the same type as in case of H_2 adsorbed on graphite.^{21,31} The density of this phase is determined by the mean spacing of the domain walls. Two simple examples of such structures are shown in Fig. 10. Figure 10(a) displays an idealized structure at $\rho=1.126$ with six commensurate rows per domain and with sharp walls, which represents the lattice-gas limit. As the deuterium molecules overlap, the walls have to be relaxed. This leads to the structure of Fig. 10(b) at the same density, and Fig. 10(c) at $\rho=1.092$ corresponding to eight commensurate rows per domain. Structures with a regular wall spacing can be divided into simple unit cells as is shown in the figure. The long lattice constant of the rectangular unit cell is given by the separation of neighboring domain walls and is a measure of the density of the structure. The small lattice constant is always $\sqrt{3} a_{gr}$ independent of the density, where a_{gr} is the graphite lattice spacing ($a_{gr}=2.459 \text{ \AA}$). Obviously, the relaxation of

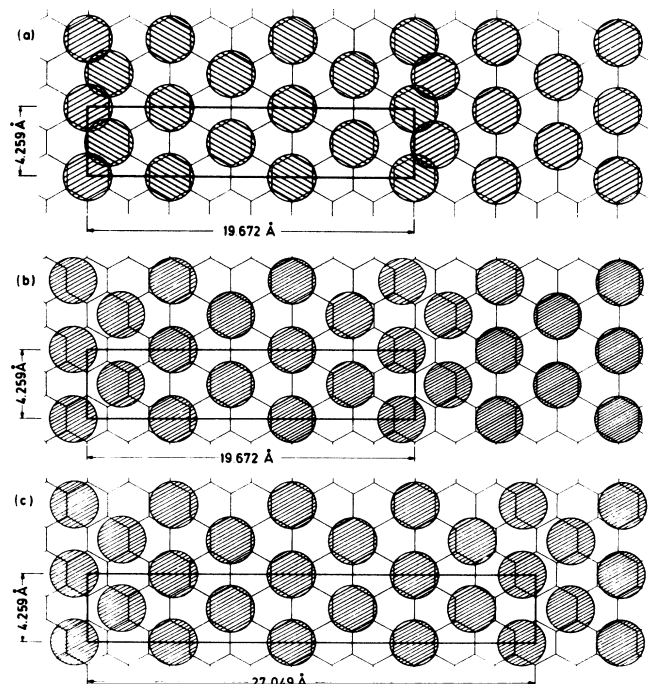


FIG. 10. Striped superheavy domain-wall structures of D_2 at two densities on a graphite basal plane. (a) Idealized structure with sharp walls at $\rho=1.126$. (b) Relaxed domain-wall structure at the same density. (c) Relaxed domain-wall structure at $\rho=1.092$. The rectangular unit cells of the structures are indicated by the solid lines. For the relaxed structures a domain wall width of $w=2.8$ is chosen (see text for details).

the domain walls does not change the size of the unit cell, and therefore it does not alter the positions of the Bragg reflections. Only the intensities of the peaks are influenced, because the structure factor depends on the exact position of all particles within the unit cell.

The inset of Fig. 11 shows a part of the reciprocal lattice of a striped domain-wall structure with superheavy walls. The lengths of the reciprocal-lattice vectors \mathbf{a}^* and \mathbf{b}^* are given by $|\mathbf{a}^*| = 2\pi/L$, where L is the domain-wall spacing of the structure, and $|\mathbf{b}^*| = 2\pi/(a_{gr}\sqrt{3})$. The open circles indicate the position of the $\sqrt{3}$ peaks. The solid circles marked by the numbers (1)–(5) give the reciprocal-lattice points of the domain-wall structure in the vicinity of the $\sqrt{3}$ -peak positions. The simple structures of Fig. 10 apply only at discrete densities and therefore yield only discrete peak positions. The continuous increase of peak splitting with density (see Figs. 4 and 11) can be explained by a model, which assumes a variation in wall separation and thus a distribution of domain sizes at each density.^{31–33,54} This size distribution might be caused by equilibrium fluctuations of domain walls³⁷ or by pinning effects at the edges of the crystallites. Extensive numerical calculations of spectra resulting from a domain-size distribution are given in Ref. 33.

In Fig. 11 the calculated positions of the Bragg reflections of striped superheavy domain-wall structures (solid lines) are compared with the experimental data for D_2 and H_2 /graphite. The single commensurate peak at $Q_C = 1.703 \text{ \AA}^{-1}$ and at $\rho \leq 1$ splits up into several components (1)–(5) (see peak designation of the inset) at $\rho > 1$. An overfilling of the C phase of about 2% is observed before the main peak shifts away from Q_C . For D_2 as for H_2 /graphite satellites can be resolved at $\rho \gtrsim 1.05$. The two components of the lower- Q satellite (1) and (2) cannot be resolved due to their low intensities and because the magnitude of the Q vectors associated with them are very close. The higher- Q satellite (4) is partly hidden by the (002)-graphite reflection and cannot be located with sufficient accuracy to be compared with the model for $\rho \lesssim 1.12$. The intensity of component (5) in Fig. 11 and of all other possible reflections in the experimentally observed Q space is too small to be detected. The error bars of the low- Q satellite [(1)+(2)] are caused by its small intensity, whereas for the high- Q satellite (4) the uncertainty in locating the peak is due to the interference with the (002)-graphite peak. Errors in the position of the main peak (3) are smaller than the symbol sizes.

The ratio of the intensity of the satellite to the intensity of the main peak gives information about the relaxation of the superheavy walls. In unrelaxed structures the Bragg points (1) and (3) have always equal intensity. With increasing relaxation the intensity of reflections (1) and (2) decreases, whereas the intensity of (4) increases. In a uniformly compressed structure only peaks (3) and (4) would remain. Unfortunately, the observation of peak (4) is mostly hindered by the (002)-graphite reflection, so that only the lower- Q satellite [(1)+(2)] can be used for a quantitative analysis of the relaxation of the domain walls.

Figure 12 shows the ratio of the square of the structure factors $|F_{\text{sat}}|^2/|F_{\text{main}}|^2$ of satellites (1)+(2) to main peak (3) vs density for D_2 /Papyex (crosses), D_2 /ZYX graphite (open triangles), and H_2 /Papyex (solid circles) at $T = 2 \text{ K}$. The solid lines give the results of model calculations for different domain-wall widths $w = 2.5, 2.8, \text{ and } 3.0$ (see text for details). The fair agreement between theoretical and experimental results provides strong support for the interpretation of the α phase as a striped superheavy domain-wall phase.

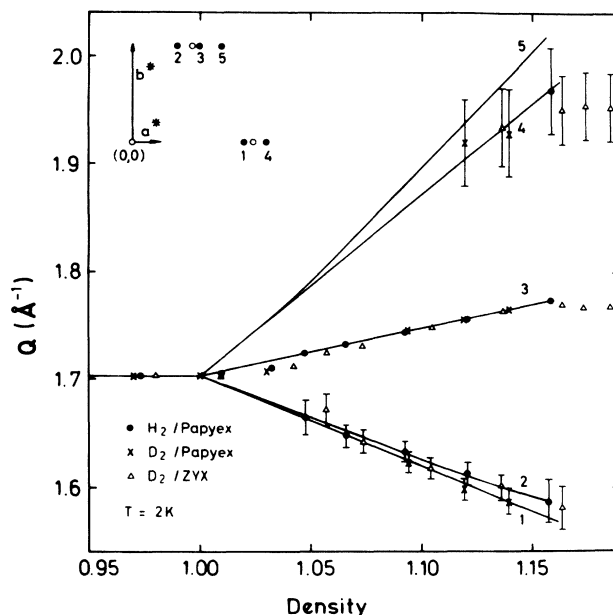


FIG. 11. Comparison of predicted positions (solid lines) with observed positions of neutron-diffraction peaks for D_2 and H_2 adsorbed on graphite at $T = 2 \text{ K}$. The inset shows a part of the reciprocal lattice of a striped domain-wall structure. \mathbf{a}^* and \mathbf{b}^* are reciprocal-lattice primitive vectors. The specular peak in the inset is denoted by (0,0). The solid circles indicate satellite reflections, marked by numbers (1), (2), (4), and (5), and the main Bragg reflection (3) in the vicinity of the commensurate $\sqrt{3}$ peak (open circles). The interpretation of the α phase as a striped superheavy domain-wall phase (solid lines) gives an excellent description of the experimental data as well for D_2 /Papyex (crosses) and D_2 /ZYX graphite (open triangles) as for H_2 /Papyex (solid circles).

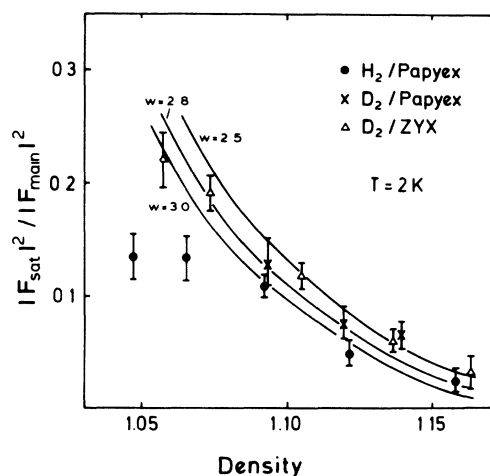


FIG. 12. Ratio of the square of the structure factors $|F_{\text{sat}}|^2/|F_{\text{main}}|^2$ of satellite peaks (1)+(2) to main peak (3) vs density for D_2 /Papyex (crosses), D_2 /ZYX graphite (open triangles), and H_2 /Papyex (solid circles) at $T = 2 \text{ K}$. The solid lines give the results of model calculations for different domain-wall widths $w = 2.5, 2.8, \text{ and } 3.0$ (see text for details). The fair agreement between theoretical and experimental results provides strong support for the interpretation of the α phase as a striped superheavy domain-wall phase.

(3) as a function of density for D_2 /Papyex, D_2 /ZYX, and H_2 /Papyex at $T=2$ K. Hereby the structure factors were deduced from the observed peak intensities according to Eq. (1) by considering the Debye-Waller factor, the Lorentz factor, the molecular form factor, and the multiplicities of the reflections. The structure factor of the satellite F_{sat} contains the contributions of both reflections (1) and (2), which cannot be experimentally separated, and their multiplicity ($|F_{\text{sat}}|^2 = 2|F(1)|^2 + 4|F(2)|^2$). The multiplicity is also considered in the structure factor of the main peak (3): $|F_{\text{main}}|^2 = 4|F(3)|^2$. In order to describe the experimental data of Fig. 12, one has to make an assumption on the relative positions of the molecules inside the unit cell. For that purpose we used the domain-wall profile derived by Gordon and Lançon.⁵⁵ The displacement $u(n)$ of the n th particle row perpendicular to the wall is given by

$$u(n) = -(4b_x/3\pi)\tan^{-1}\{\exp[(n-\alpha)\pi/w]\}, \quad (3)$$

where b_x is the separation of two commensurate rows and $\alpha = \frac{1}{2}$ for noncentered walls. w is a measure of the domain-wall width in the units of molecular row spacing in the C phase. Calculating structure factors by applying this relation results in the solid lines of Fig. 12 for three different values $w=2.5, 2.8$, and 3.0 of the wall width. All data for D_2 and H_2 follow essentially the same curve, there is no difference between data taken on Papyex or ZYX graphite. The D_2 data seem to point to somewhat sharper walls ($w \approx 2.5-2.8$) than the H_2 data ($w \approx 2.8-3.0$). As the complete D_2 monolayer due to the reduced zero-point energy is packed closer than the complete H_2 monolayer, this tendency is reasonable. At low densities the H_2 data deviate from the theoretical curves, because in this range satellite and main peak already overlap, and it is difficult to determine the intensity of the satellite separately. For D_2 on ZYX the situation is better due to the higher diameters of the substrate crystallites.

Although the determination of the intensity of the high- Q satellite (4) is rather uncertain due to the strong influence of the (002)-graphite reflection, the ratio $I_{\text{main}}/I(4)$ is $\approx 2-3$ at $\rho=1.13$ in good agreement with the calculated value of this ratio of ≈ 2.5 for a wall width of $w=2.5$.

The domain-wall widths found from the present analysis are strongly supported by recent variational calculations by Gottlieb and Bruch⁵² based on a multiparameter potential model. These calculations of the energy and structure of uniaxially incommensurate monolayer lattices of D_2 and H_2 give a fairly good account of our experimental data. The relatively sharp walls observed for the hydrogen isotopes are a consequence of the high compressibility of these 2D quantum solids. For illustration real-space structures with a domain-wall width of $w=2.8$ are shown in Figs. 10(b) and 10(c). Essentially four particle rows are influenced near a domain wall, the next rows at a wall are displaced by $a_{\text{gr}}/3$ and the next nearest by $a_{\text{gr}}/10$ from their commensurate sites.

Figures 1, 4, and 11 show an overfilling of the complete commensurate phase of D_2 as of H_2 of a few percent.

Hereby the coherence lengths of the C peaks diminish to values of about 100 Å indicating a strong disturbance of the $\sqrt{3}$ structure by interstitials. The first signatures of satellite peaks only appear at $\rho \geq 1.05$ and the α phase is formed. This behavior can be easily interpreted on the basis of the domain-wall model, because a minimum of additional particles is needed to form a domain wall and a minimum number of domain walls per graphite crystallite is needed to result in an observable diffraction pattern. The lowest density yielding a resolvable satellite corresponds to a structure with 14 commensurate rows per domain, which leads to five to six domain walls per Papyex crystallite of about 250-Å diameter. This is probably near the minimum number of walls for which a satellite structure is observable on Papyex.

The phase transition from the commensurate phase to the striped domain-wall phase seems to be continuous. No discontinuous jump of the peak positions or a coexistence region of the C and the α phases indicating a first-order transition could be detected within experimental accuracy. The occurrence of a second-order transition from the commensurate to the striped domain-wall phase is consistent with theoretical predictions.^{5,7}

As was discussed in Ref. 31, the upper density limit of the α phase of H_2 /graphite is near $\rho \approx 1.16$. This seems reasonable because at this density only four to five commensurate rows remain per domain and four of these are involved in the relaxation process of the walls. As the relaxation is very similar for H_2 and D_2 , the same upper density limit is plausible. In the case of H_2 /graphite the α phase is followed by a narrow region of the β phase and the IC phase (see phase diagram, Fig. 1). For D_2 /graphite the situation is quite different. Beyond $\rho \approx 1.16$ the α phase undergoes a first-order phase transition via a coexistence region into a new type of solid, the γ phase.

V. THE γ PHASE

The γ phase represents a new 2D crystalline solid state, which has not been observed for any other system before. The striking feature of the γ phase is that the main peak is always at the position of the (10) peak of an equilateral triangular IC structure of the same density (see Fig. 4). In addition, satellites were observed on both sides of the main reflection (Figs. 3, 8, and 9). In principle, this behavior can be explained by assuming the γ phase to be a density-modulated equilateral triangular IC phase. In the limit of weak substrate modulation such a phase can be described by the Novaco-McTague theory,¹ which takes into account only linear contributions of the substrate field and which therefore leads to pure sinusoidal density-modulation waves. This theory has been very successful in explaining the rotational epitaxy of weakly modulated IC phases.^{36,37,56} However, in these phases, as, e.g., in the IC phases of H_2 and D_2 on graphite of the present work, no modulation satellites could be detected in diffraction experiments,^{41,57} because the density modulations are too weak. The observation of satellite peaks in the γ phase indicates that the modulation in this phase is stronger. This is also supported by LEED

results,^{36,37} where a completely different rotational epitaxy was found for the γ phase than for the IC phase. At present there are no continuum model calculations of 2D quantum solids available, which consider nonlinear terms and account for stronger modulations. The most complete theory is that of Shiba,⁵⁸ but this may not be valid for our system, because the influence of large zero-point motions is not taken into account. Due to this lack we had to resort to a harmonic distortion theory of the kind also applied to 3D systems.^{59,60} We show in this section that this linear theory—even being considered only as a first approximation—provides a good agreement with experimental data.

Figure 13 displays part of the reciprocal space of a modulated structure. In addition to peak (4) of the unmodulated structure with wave vector τ_{10} , a star of six satellites of first order arises due to the density modulation of the adsorbate by the periodic substrate field with hexagonal symmetry. The peaks are marked by numbers (1)–(7), which are put in order of the magnitudes of their associated wave vectors. The satellite peaks are located at positions $\mathbf{Q}=\tau+\mathbf{q}$, where $\mathbf{q}=\mathbf{G}-\tau$ with \mathbf{G} being a first-order graphite reciprocal-lattice vector. In the LEED measurements^{36,37} the modulation wave vector \mathbf{q} was found to be parallel to one of the equivalent (100)-graphite vectors, as indicated in Fig. 13 [arrow pointing from the (11) overlayer to the graphite (100) reflection]. The dashed line represents the wave vector of the commensurate $\sqrt{3}$ structure \mathbf{Q}_C . The wave vector τ_{10} of the main reflection (4) is rotated by the angle θ with respect to \mathbf{Q}_C . This angle cannot be determined in a neutron-diffraction measurement because of the powder nature of

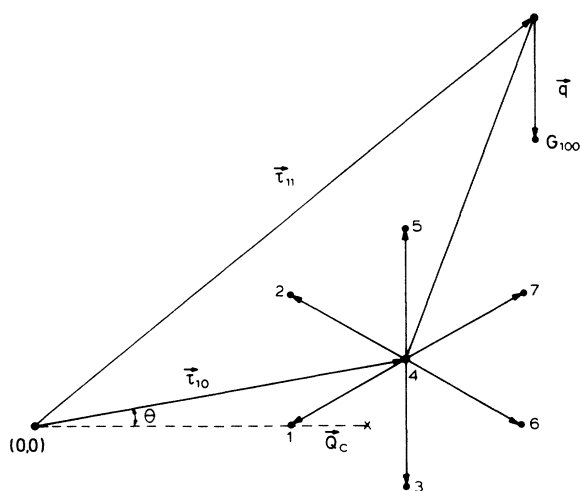


FIG. 13. A reciprocal-space diagram of the density-modulated γ phase. The specular peak is denoted by (0,0). In addition to the main peak (4) with wave vector τ_{10} , six satellite peaks (1)–(3), (5)–(7) appear, which are constructed by adding the modulation wave vector \mathbf{q} to τ_{10} . According to LEED results (Refs. 36 and 37) \mathbf{q} always points into a graphite high-symmetry direction. The adsorbate is rotated by the angle θ with respect to the lattice-vector \mathbf{Q}_C of the commensurate $\sqrt{3}$ phase.

the employed pyrolytic graphite substrate. However, in LEED experiments of Cui and Fain^{36,37} on single graphite crystals it turned out to be between $\theta=7^\circ-11^\circ$ at $\rho=1.18-1.31$, much bigger than in the uniformly compressed IC phase at higher densities. Based on this result the structure of the γ phase can be determined at each density.

Figure 14 illustrates, for example, the structure of the γ phase at $\rho=1.28$. The D_2 molecules are arranged in an equilateral triangular IC structure rotated by the angle θ away from the $\sqrt{3}$ -phase orientation. The unit cell is given by the solid lines. Due to the presence of the lateral substrate modulation potential periodic strains will be exerted on the overlayer and a static distortion wave is generated. Its modulation length can be inferred from the magnitude of the modulation vector \mathbf{q} by $L=2\pi/[q \sin(60^\circ)]$. Two modulation cells are indicated by dashed lines in Fig. 14. The orientation of the modulation cell is parallel to a graphite [100] direction.

The nature of the modulation still has to be determined from an analysis of the peak intensities, but the positions of the Bragg reflections can already be calculated at this point. Due to the sixfold symmetry of the substrate potential, the main Bragg reflection is surrounded by six first-order overlayer reflections (1)–(3), (5)–(7). This is a so-called triple- q structure. Peaks (3) and (4) coincide in a neutron-diffraction experiment because of equal absolute values of $|\mathbf{Q}|$. The satellites (6) and (7) are located between $|\mathbf{Q}|\approx 2.3-2.6 \text{ \AA}^{-1}$ and could not be detected in the experiment. The rest of the satellites (1)–(5) have been observed and their positions are plotted in Fig. 15 as a function of density. The solid lines represent the results of the calculations, which are in excellent agreement with the experimental data of all reflections found.

In order to estimate the intensity of the observed peaks, it is necessary to assume a model about the kind of the density modulation. To minimize their energy the adsorbed molecules will tend to move towards the centers of the nearest graphite hexagons. This is indicated by the

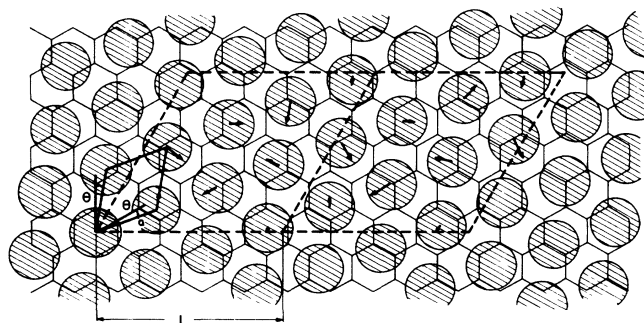


FIG. 14. The structure of the γ phase at $\rho=1.28$ on a graphite basal plane. The solid lines indicate the unit cell with lattice constant a of the uniformly compressed phase, which is rotated by the angle θ with respect to the commensurate $\sqrt{3}$ direction. The dashed lines represent two modulation cells with side length L . The arrows indicate the direction of forces exerted on the molecules by the lateral substrate corrugation potential.

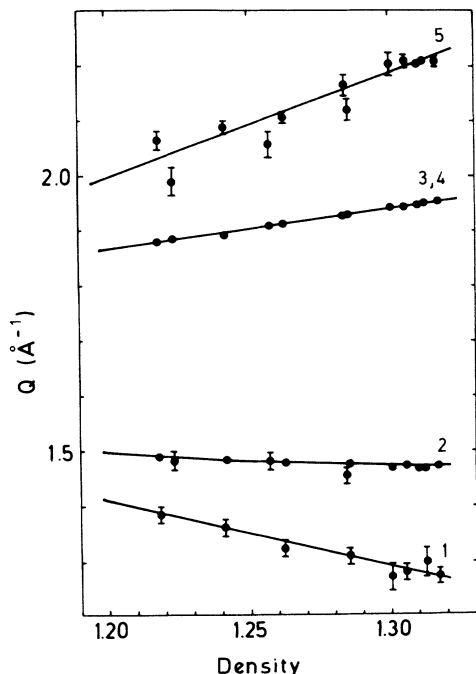


FIG. 15. The position (Q) of diffraction peaks (1)–(5) from the γ phase vs density at $T=2$ K. The solid lines were calculated by assuming a static strain modulation of the adsorbate, which provides a perfect description of the experimental data (solid circles) in the total density range.

arrows in Fig. 14, which represent the forces on the single particles experienced by the lateral graphite corrugation potential. Due to the different positions of the D_2 molecules in each modulation cell, the pattern of the arrows is different as well. Superposing the patterns of many modulation cells, however, results in a homogeneous picture as is shown in Fig. 16. Consequently, the displacement of a molecule due to the density modulation is unambiguously given by its position inside a modulation

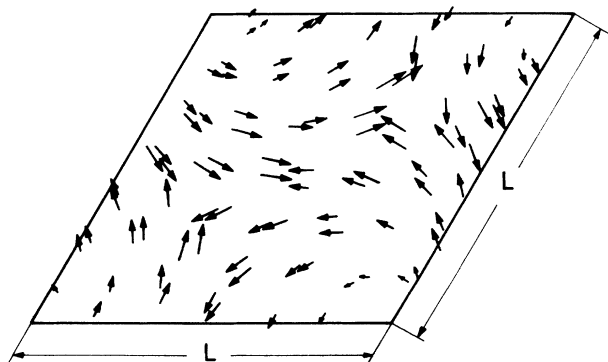


FIG. 16. Displacement pattern of molecules resulting from the superposition of many modulation cells of the kind shown in Fig. 14. The arrows indicate the forces experienced on the molecules by the corrugation potential of the substrate and illustrate the formation of static distortion waves.

cell. The actual modulation of the structure should yield a similar picture except for the long arrows in Figs. 14 and 16, which will be significantly shortened. The long arrows, i.e., strong forces, appear where molecules are far away from the centers of graphite hexagons. Releasing the strain by moving to the next commensurate sites results in a conflict with the hard-core repulsive forces between the molecules because adjacent hexagon centers cannot be occupied due to the size of the molecules. Therefore, in these cases the actual displacements will be smaller than those indicated by the long arrows in Figs. 14 and 16. From the modulation patterns of Figs. 14 and 16 one may conclude that the modulation of the γ phase can be described in first approximation by sinusoidal distortion waves propagating along the graphite [100] direction. The amplitude U of the sine wave is a vector rotated by 60° from the direction of propagation. The length of the vector must be chosen in the way that the calculated intensity ratios $I_{\text{sat}}/I_{\text{main}}$ fit the experimental data. A similar displacement pattern as in Fig. 16 was found by Shiba⁵⁸ studying the effect of the graphite substrate potential on IC monolayers of heavy rare gases.

The structure factor of the modulated phase is given by^{1,59,60}

$$F(\mathbf{Q}) \sim \prod_{\mathbf{G}} J_0(\mathbf{Q} \cdot \mathbf{U}_{\mathbf{G}}) \Delta(\mathbf{Q}) + 2 \sum_{\mathbf{G}_1} \left[\prod_{\mathbf{G} \neq \mathbf{G}_1} J_0(\mathbf{Q} \cdot \mathbf{U}_{\mathbf{G}}) \right] J_1(\mathbf{Q} \cdot \mathbf{U}_{\mathbf{G}}) \Delta(\mathbf{Q} + \mathbf{G}_1), \quad (4)$$

where J_0 and J_1 are the Bessel functions of the first kind, $\Delta(\mathbf{Q})$ is the periodic δ function given by $\Delta(\mathbf{Q}) = \sum_{\boldsymbol{\tau}} \delta_{\mathbf{Q}, \boldsymbol{\tau}}$ with $\boldsymbol{\tau}$ being a reciprocal-lattice vector of the undisturbed structure (see Fig. 13). \mathbf{G} and \mathbf{G}_1 are reciprocal-lattice vectors of the substrate, and $\mathbf{U}_{\mathbf{G}}$ is the amplitude of the modulation along a graphite high-symmetry direction. As the argument of the Bessel function is small, J_0 is always near unity and the intensity of the satellite reflections is essentially given by $|J_1(\mathbf{Q} \cdot \mathbf{U}_{\mathbf{G}})|^2$.

In Table I the positions of all Bragg reflections at the investigated densities of the γ phase, the observed intensity ratios of the satellites to the main peak $I(Q_{\text{sat}})/I(Q_{\text{main}})$, and the absolute values of the squares of the structure factor ratios

$$|F(Q_{\text{sat}})|^2 / |F(Q_{\text{main}})|^2$$

are compiled. The structure factors have been obtained from the intensities according to Eq. (1) by considering the contributions of the Debye-Waller factor, the Lorentz factor, and the molecular form factor. As the Bragg reflections of the γ phase are spread over a relatively large Q range ($1.2 \leq Q \leq 2.3 \text{ \AA}^{-1}$), the influence of these factors is appreciable as can be seen by comparing the data given in the table. The structure factors of satellites (1) and (2) lose and that of satellite (5) gains in magnitude compared with the main peak.

Figure 17 shows the comparison of the experimental data found for the squares of the structure factor ratios and the calculations according to (4) for a density modu-

TABLE I. Experimental data of the wave vectors of main (4) and satellite peaks (1), (2), and (5) at the studied densities of the γ phase. $I(Q_{\text{sat}})/I(Q_{\text{main}})$ are the measured intensity ratios of the corresponding peaks and $|F(Q_{\text{sat}})|^2/|F(Q_{\text{main}})|^2$ are the squares of their structure factor ratios. The latter data are calculated from the intensities according to Eq. (1) by taking into account values of the Debye-Waller factor, the Lorentz factor, and the molecular form factor. The asterisks indicate peak positions and intensities which could not be determined.

ρ	$Q_{\text{main}} (\text{\AA}^{-1})$	$Q_1 (\text{\AA}^{-1})$	$\frac{I(Q_1)}{I(Q_{\text{main}})}$	$\frac{ F(Q_1) ^2}{ F(Q_{\text{main}}) ^2}$	$Q_2 (\text{\AA}^{-1})$	$\frac{I(Q_2)}{I(Q_{\text{main}})}$	$\frac{ F(Q_2) ^2}{ F(Q_{\text{main}}) ^2}$	$Q_5 (\text{\AA}^{-1})$	$\frac{I(Q_5)}{I(Q_{\text{main}})}$	$\frac{ F(Q_5) ^2}{ F(Q_{\text{main}}) ^2}$
1.317	1.954	1.277	0.015	0.006	1.472	0.051	0.025	2.206	0.045	0.064
1.312	1.952	1.29	0.026	0.011	1.468	0.054	0.027	2.209	0.053	0.077
1.310	1.949	*	*	*	1.468	0.058	0.029	2.205	0.046	0.065
1.305	1.946	1.283	0.020	0.008	1.474	0.066	0.033	2.208	0.051	0.075
1.285	1.928	1.310	0.023	0.009	1.477	0.063	0.032	2.121	0.054	0.071
1.284	1.930	*	*	*	1.455	0.045	0.023	2.165	*	*
1.262	1.913	1.323	0.033	0.014	1.481	0.069	0.037	2.105	0.056	0.074
1.257	1.910	*	*	*	1.482	0.060	0.032	2.058	*	*
1.241	1.889	1.360	0.028	0.012	1.485	0.071	0.039	2.088	0.053	0.072
1.223	1.884	*	*	*	1.479	0.066	0.036	1.991	*	*
1.218	1.882	1.385	0.023	0.011	1.489	0.045	0.025	2.065	0.053	0.070

lated structure (solid lines). To fit the data we used an amplitude of modulation of $|\mathbf{U}|=0.14 \text{ \AA}$. Evidently there is an overall good agreement between observed and calculated data. At higher densities $\rho \geq 1.30$ there is a slight tendency of the observed satellite intensities to deviate to somewhat lower values from the calculated lines. This may be easily explained by assuming a smaller modulation amplitude in the closer-packed structures near the upper density limit of the γ phase.

The angle between the amplitude \mathbf{U} and the direction of propagation of the modulation was assumed to be 60° as mentioned above. The modulation vector \mathbf{q} is there-

fore always perpendicular to $\mathbf{U}(\mathbf{q})$. This choice seems reasonable by considering Fig. 16. An analysis of the influence of the variation of this angle on the intensity ratio shows that it has an important effect. In order to get a reasonable description of the experimental results, the angle is not allowed to be varied by more than $\pm 3^\circ$. Thus, one can infer from the intensities of the satellites that the amplitude of displacement \mathbf{U} is always along a graphite high-symmetry direction in real space. This provides besides the observation from LEED,^{36,37} that the modulation wave vector \mathbf{q} also points into a graphite symmetry direction in reciprocal space, an important clue for the understanding of the γ phase.

From the analysis presented here one may conclude that the interpretation of the γ phase as a density-modulated phase is consistent with experimental data. In the next section we will work out that the topological structure of the γ phase is analogous to that of a hexagonal heavy domain-wall phase.

VI. THE δ AND ϵ PHASES

The δ and ϵ phases denote two regions of the D_2 /graphite phase diagram, which could be unambiguously detected by the observation of anomalies in specific-heat measurements^{21,24,25} [see Fig. 1(a)]. On the other hand, in neutron-diffraction measurements no discontinuities of any kind could be found to identify these phases, neither as concerns the peak positions (Figs. 4 and 15) nor the structure factor ratios (Fig. 17). The γ phase behaves like a single phase throughout its whole density region. In order to understand this apparently inconsistent behavior, one has to look at the structure of the γ phase more closely.

Near the upper density limit of the γ phase at $\rho=1.313$, where specific-heat measurements have discovered the ϵ phase, the modulation length L equals four times the lattice constant a_{gr} and the modulated structure becomes a higher-order commensurate (4×4) structure. At this particular density also the rotation an-

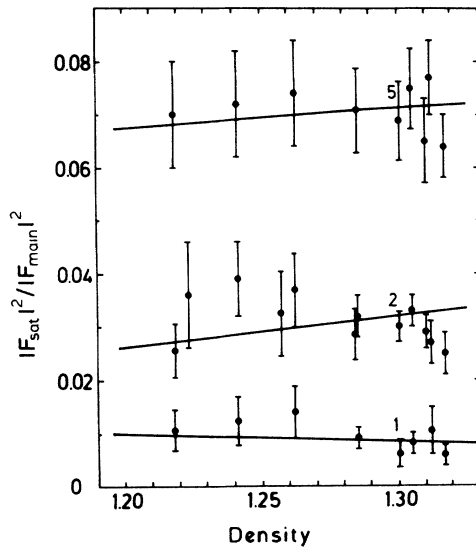


FIG. 17. The squares of the structure factor ratios of satellites (1), (2), and (5) to main peak vs density at $T=2 \text{ K}$. The solid lines represent the results of the calculations according to Eq. (4). The good agreement between experiment and theory supports the interpretation of the γ phase as a density-modulated phase.

gle of the adsorbate^{36,37} adjusts in a way that this structure is formed. Figure 18(a) (upper panel) illustrates the uniformly compressed (4×4) structure. It can be seen that for this special structure the unit cell coincides with the modulation cell (heavy solid line). It contains seven molecules, which still are affected by the periodic corrugation field of the substrate leading to density modulations. Figure 18(b) (lower panel) shows the extreme modulation limit, when all particles are shifted to the centers of their next graphite hexagons. Schematically the occupied sites are indicated by hatched hexagons. Evidently a hexagonal heavy domain-wall network with sharp walls is formed. As the molecules would overlap in this idealized structure, the walls still have to be relaxed. This results in a density-modulated structure of the kind treated in Sec. V and elucidates that both of the structures are, in fact, equivalent.

The (4×4) structure is the simplest higher-order commensurate structure, which is identical with the density-modulated γ phase. In the case of $L = 5a_{gr}$ and $6a_{gr}$ no commensurate (5×5) and (6×6) structures, respectively, occur, because they do not fit to the special rotational epitaxy of the γ phase. At $L = 7a_{gr}$ the modulated struc-

ture describes a (7×7) phase, which can also be considered as a hexagonal heavy domain-wall phase. However, the density of the (7×7) structure is $\rho = 1.163$ just outside the region of the γ phase.

The next simple higher-order commensurate phases identical with the modulated structure in the density range of the γ phase are the ($5\sqrt{3}\times 5\sqrt{3}$) structure at $\rho = 1.240$ and the ($6\sqrt{3}\times 6\sqrt{3}$) structure at $\rho = 1.194$. The uniformly compressed ($5\sqrt{3}\times 5\sqrt{3}$) structure is shown in Fig. 19(a). The modulation cell with $L = 5a_{gr}$ is indicated by the dashed line and the unit cell containing 31 particles by the solid line. Figure 19(b) displays a schematic representation of this structure as idealized hexagonal heavy domain-wall structure with sharp walls. In relaxed form the equivalence of this structure with a density-modulated phase again becomes apparent. The density of this structure is $\rho = 1.240$. This happens to be just at that density where specific-heat measurements^{21,24,25} have found the δ phase. Therefore, it is obvious to suppose that the δ phase can be identified as commensurate ($5\sqrt{3}\times 5\sqrt{3}$) structure and—as discussed above—the ϵ phase with a commensurate (4×4) structure. It is evident that both phases cannot be dis-

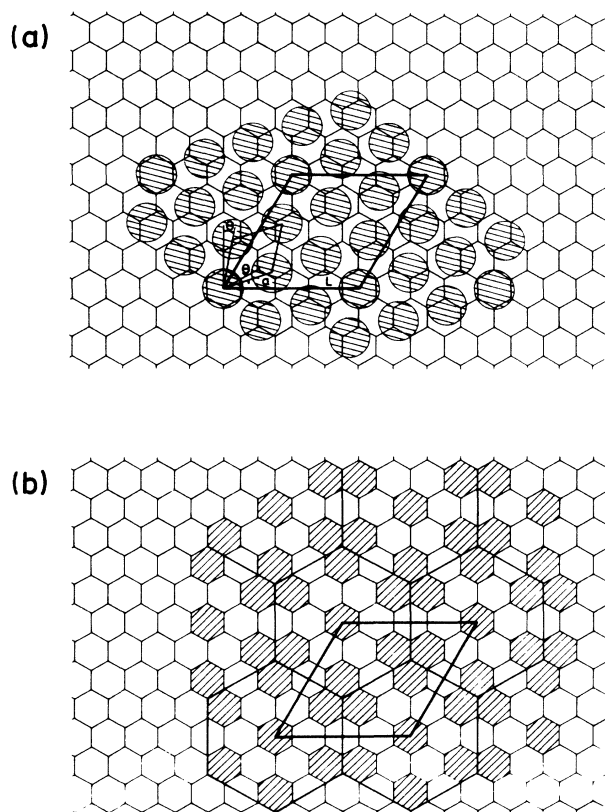


FIG. 18. The higher-order commensurate (4×4) structure at density $\rho = 1.313$ for two limiting cases of density modulation: (a) the uniformly compressed structure (upper panel) and (b) the idealized hexagonal heavy domain-wall structure (lower panel). The hatched hexagons schematically represent graphite sites occupied by molecules. The unit cell is indicated by the thick solid line. It is assumed that the ϵ phase can be regarded as density-modulated (4×4) structure.

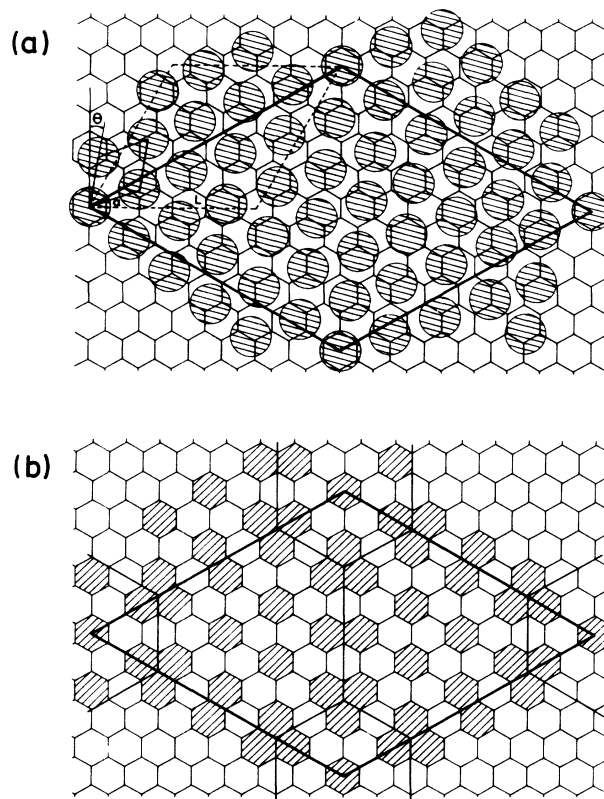


FIG. 19. The higher-order commensurate ($5\sqrt{3}\times 5\sqrt{3}$) structure at density $\rho = 1.240$ for the limiting cases of weak and strong density modulation: (a) the uniformly compressed structure. The modulation cell is given by the dashed lines and the unit cell by the solid lines. (b) The idealized hexagonal heavy domain-wall structure. The hatched hexagons indicate occupied substrate sites. It is assumed that a ($5\sqrt{3}\times 5\sqrt{3}$) structure with density modulations intermediate between these two cases might be adopted by the δ phase.

tinguished from the γ phase by examining peak positions only. Differences in the intensity ratios caused by slightly modified modulation patterns of the higher-order C phases might be very small. This explains why diffraction results cannot reveal any differences between the γ , δ , and ϵ phases.

In principle, a $(6\sqrt{3} \times 6\sqrt{3})$ phase might appear at $\rho = 1.194$. If it actually did exist, its detection by specific-heat measurements might have been missed, because its density range is probably very small and its transition temperature very low. Still higher-order commensurate phases are increasingly unlikely to appear.

VII. DISCUSSION OF THE C-IC TRANSITION

The Kosterlitz-Thouless criterion⁶¹ for a solid-solid C-IC transition is $p^2 > 8$, where p is the number of equivalent commensurate sites. In the $(\sqrt{3} \times \sqrt{3})$ structure on graphite we have $p^2 = 9$, and therefore a direct transition between a commensurate and a floating solid IC phase is possible. The low-density incommensurate phase in D_2 and H_2 adsorbed on graphite is a striped domain-wall phase (α phase) so that the hexagonal symmetry is broken. In this case Bak *et al.*⁵ predicted a second-order transition. Villain⁶ pointed out that due to entropy contributions the free energy of the hexagonal phase is lower than that of the striped phase, so that a weakly first-order transition C-hexagonal is to be expected. Coppersmith *et al.*,⁸ however, found that the order of commensurability is sufficiently low to squeeze in a narrow fluid phase down to 0 K between the commensurate and the hexagonal incommensurate phase.

The $\sqrt{3}$ phase of H_2 and D_2 /graphite undergoes a transition into a fluid phase (β phase) with increasing density, at least at higher temperatures. In the specific-heat measurements the β phase could be traced down to ≈ 6.5 K for D_2 and to ≈ 8.5 K for H_2 . The present neutron-diffraction measurements of H_2 and D_2 monolayers are consistent with a second-order solid-solid transition from a commensurate to a striped domain-wall phase (cf. Refs. 21 and 31–33). The possibility of a narrow fluid region down to 0 K cannot be ruled out totally, but its width at 2 K can be confined to less than 3 and 2% of the $\sqrt{3}$ density for H_2 and D_2 , respectively, otherwise it would have been detected. It seems more likely that the β phase terminates between 2 and 8.5 K for H_2 and between 2 and 6.5 K for D_2 as is indicated in the phase diagram by the dashed lines (Fig. 1).

A similar situation occurs for Kr/graphite, where the commensurate $\sqrt{3}$ phase is separated from a hexagonal IC phase by a reentrant fluid at least down to 80 K.⁶² As no signal of any striped phase could be detected, the C-IC transition of Kr monolayers may be first order. Corresponding experimental evidence was found by Nielsen *et al.*⁶³ at low temperatures. At higher temperatures, however, Specht *et al.*¹² found a continuous commensurate-reentrant fluid transition.

Following Halpin-Healy and Kardar,¹³ the density-temperature region of the striped phase is limited by two effects: (a) The wall crossing energy is responsible for the

maximum transition temperature. As we have $T_{\max} \approx 7.3$ K for D_2 and $T_{\max} \approx 9.7$ K for H_2 , wall crossings in H_2 should be energetically more unfavorable than in D_2 . This seems reasonable, because a hexagonal domain-wall phase could not be observed in H_2 monolayers. (b) The strength of the wall repulsion determines the upper density limit of the striped phase. The exponential decay of the wall repulsion is characterized by the wall thickness λ_0 , where λ_0 is given by $\lambda_0 = w/\pi$ [w is the wall thickness according to Eq. (3)]. From our determined structure factor ratios $|F_{\text{sat}}|^2/|F_{\text{main}}|^2$ in the α phase (Fig. 12), we conclude that H_2 and D_2 have approximately equal wall widths within experimental uncertainty. This explains why the α phase of both systems vanishes at nearly the same density.

The absence of a striped phase in Kr monolayers can be understood as resulting from the large wall thickness $\lambda_0 \approx 5$ ($w \approx 16$),⁶⁴ which enhances the wall repulsion leading to an instability of the striped phase to the formation of a hexagonal phase.¹³ The hydrogen isotopes reveal considerably sharper walls corresponding to $\lambda_0 \approx 0.8$ – 0.9 . The upper density limit of the striped phase of both isotopes turned out to be $\rho \approx 1.16$. Theoretical results of Halpin-Healy and Kardar¹³ for $\lambda_0 = 1$ yield a striped phase up to $\rho = 1.24$, a hexagonal phase at $\rho \geq 1.29$, and a coexistence region in between.

The melting of the striped phase (α phase) is expected to belong to the Kosterlitz-Thouless universality class.¹³ A small but growing population of wall crossings is sufficient to disorder the striped phase as the temperature is raised. The reentrant fluid (β phase) may then be described as a disordered network of domain walls, a domain-wall fluid. According to diffraction data, the β phase is a well-correlated fluid. On melting for D_2 a discontinuous jump of the Q vector to that of an equilateral triangular IC phase of the same density was observed, whereas for H_2 no such anomaly was found (Fig. 7). Recently inelastic neutron-diffraction measurements by Frank *et al.*^{35,65} proved that the β phase is a disordered domain-wall phase, because excitations of the C phase and excitations attributed to the domain walls of the α phase could also be detected in the β phase. LEED (Refs. 36 and 37) at $\rho \approx 1.15$ has revealed that the β phase of D_2 has the same rotational epitaxy as the γ phase. Therefore, the β phase may be considered as a molten γ phase at least at coverages not too close to the commensurate phase. The β phase of H_2 , on the other hand, is aligned along the $\sqrt{3}$ direction of the substrate as is the α phase,^{36,37} so that it looks like a molten α phase. The β phases of H_2 and D_2 adsorbed on graphite seem to be different phases. In the domain-wall picture one can realize that the β phase of D_2 is dominated by an irregular pattern of hexagonal heavy domain walls, whereas for H_2 it is determined by an irregular pattern of striped superheavy domain walls containing lattice defects and wall crossings. Based on this view, the different melting behavior of the α phase of the two systems may be understood. In D_2 monolayers the specific-heat anomaly associated with the melting of the α phase is very sharp at $\rho \approx 1.1$,^{21,66} and the Bragg peak position seems to jump

discontinuously to the position of an equilateral triangular phase. These experimental facts may be understood as signaling a first-order α - β transition, which undergoes the same symmetry breaking as the first-order α - γ transition. Contrary to that, the specific-heat anomalies of the α - β transition of $\text{H}_2/\text{graphite}$ ^{18-21,66} are much more rounded and the position of the Bragg reflection remains unchanged at melting. In this case the transition is more likely to be continuous.

The interpretation of the β phase as a domain-wall fluid is supported by molecular-dynamics simulations of Abraham *et al.*,⁶⁷ who have found a disordered meandering hexagonal array of domain walls in the reentrant fluid phase of $\text{Kr}/\text{graphite}$. In a computer simulation by use of the Feynman path-integral Monte Carlo method for $^3\text{He}/\text{graphite}$,⁶⁸ which took the quantum effects into account, only a striped domain-wall fluid was observed. The system, however, was rather small containing no more than about 40 atoms.

In agreement with theoretical work,^{5,13} the transition striped (α phase)-hexagonal (γ phase) is first order. The coexistence region has a width of $\approx 2.5\%$ of the $\sqrt{3}$ density, which is half the value of Halpin-Healy and Kardar's calculation¹³ for He. It has to be noted, however, that their hexagonal phase is a domain-wall phase with superheavy walls, whereas the γ phase of D_2 monolayers can be described as a heavy domain-wall phase. A similar C-IC transition as in $\text{D}_2/\text{graphite}$ has been observed in Xe physisorbed on $\text{Pt}(111)$.¹⁴ Xe forms a $(\sqrt{3} \times \sqrt{3})$ structure, which undergoes a continuous transition into a striped phase followed by a first-order transition into a hexagonal phase as the misfit is increased. The width in density of the coexistence region in this case is $\approx 1.5\%$. In contrast to $\text{D}_2/\text{graphite}$, only one hexagonal phase is found and no higher-order commensurate phases are observed.

Hexagonal IC structures are expected to rotate away from the graphite symmetry directions.^{1,58,69} Such rotation cannot be seen in a powder experiment like our neutron-diffraction study. LEED measurements on a single crystal,^{36,37} however, revealed that the γ -phase rotates by an angle too large to be consistent with theoretical results for a free floating solid with central forces,¹ but it is explainable in terms of a density-modulated structure equivalent with a heavy domain-wall structure. The special rotational behavior seems to be a consequence of the reduced zero-point energy for D_2 compared to H_2 , which causes enhanced adsorbate-substrate interactions. The γ phase of $\text{D}_2/\text{graphite}$ is a new type of an IC solid which has not been observed in any other system so far.

As discussed in Sec. VI, the special rotational behavior of the γ phase is responsible for the coincidence of the modulated structure with higher-order commensurate structures. The difference between the δ and the γ phases occurring at the same density might be only that the δ phase is locked into the lattice periodicity of the substrate potential, whereas the γ phase is a nearly free-floating phase. The peak positions will not be influenced by the transition between both phases, and their peak intensity ratios might change very little. The line shapes of

the peaks, on the other hand, should be modified. The algebraic decay of correlations in the free-floating γ phase will be reflected by a power-law line shape,⁴⁶ whereas the higher-order commensurate δ and ϵ phases should possess long-range order and the line shapes should be Gaussian. The difference, however, might be marginally small, because the exponent η describing the power-law singularity of the line shape is estimated to be approximately 0.01 (Refs. 33 and 43) due to the relatively large rigidity of the IC phase of D_2 . This implies that the line shape of the γ phase might become nearly Gaussian.⁴⁶ A criterion to establish the existence of higher-order C phases is the observation of the absence of thermal expansion in the proposed C phase as has been done for $\text{Kr}/\text{Pt}(111)$ (Ref. 70) and $\text{CF}_3\text{Cl}/\text{graphite}$.⁷¹ The floating γ and equilateral triangular IC phases should, in principle, show thermal expansion, whereas the δ and ϵ phases should not. Unfortunately, the peak shift with increasing temperature is not significant within experimental error in all four phases to yield a conclusive result.

As mentioned above, the γ - δ and γ - ϵ transitions have not been seen in diffraction spectra. From specific-heat data, however, the phase boundaries could be determined. The evolution of a double peak at the γ - ϵ transition^{21,24,25} at $\rho = 1.30$ can be understood as a signal of a coexistence of γ and ϵ phases at $T < 9$ K and of ϵ and equilateral triangular IC phases between 9 and 10 K [cf. Fig. 1(a)]. This would imply a first-order γ - ϵ transition. As the δ phase is similar to the ϵ phase, the γ - δ transition should be of the same type as the γ - ϵ transition. The phase boundary of the δ phase, however, is strongly curved suggesting the absence of a coexistence of δ and γ , and therefore it implies no first-order transition. Alternatively, the phase diagram can be drawn as done in Ref. 37 with only a coexistence region of ϵ and triangular IC phases and a continuous γ - ϵ transition.

In LEED measurements^{36,37} a first-order transition from the ϵ phase to the equilateral triangular IC phase was observed. No sign of any coexistence of these two phases could be detected, neither in neutron-diffraction nor in specific-heat experiments. At $\rho \geq 1.33$ the equilateral triangular IC phase is the only stable solid phase. As is shown by LEED, it reveals a rotation angle in agreement with the predictions of the Novaco-McTague theory¹ like triangular IC solids in other systems such as H_2 ,³⁷ HD ,³⁷ and Ar .⁵⁶

In the system $\text{H}_2/\text{graphite}$, the triangular IC phase succeeds the striped α phase with a narrow fluid range in between both phases.¹⁸⁻²¹ Recent specific-heat measurements^{21,66} have revealed that the phase diagram of $\text{HD}/\text{graphite}$ is topologically similar to the $\text{H}_2/\text{graphite}$ phase diagram. A detailed study of the α -IC transition, however, yielded a series of anomalies at $T \approx 5$ K, which may indicate the existence of a triple line with α +IC coexistence below and the β phase above. This means a first-order striped hexagonal transition in agreement with theory as in the case of D_2 . It cannot be excluded that a similar behavior might occur for $\text{H}_2/\text{graphite}$ at lower temperatures ($T < 4$ K) outside the temperature range studied by specific-heat experiments.¹⁸⁻²¹

VIII. CONCLUSION

Deuterium monolayers physisorbed on the basal plane of graphite reveal the most detailed commensurate-incommensurate transition of all physisorbed systems investigated so far. It is the first system in which diffraction satellites of a striped as well as of a hexagonal array of domain walls could be observed. The surprising appearance of the γ , δ , and ϵ phases has to be attributed to the reduced zero-point energy of the D_2 molecule compared with H_2 . This leads to smaller effective sizes of the D_2 molecules resulting in a reduced wall-crossing energy making a hexagonal network of domain walls possible. Therefore, we have the unique sequence of the following: (a) A high-density IC phase at $\rho \geq 1.33$, which shows little influence of the graphite substrate, so that the harmonic description of the periodic distortions of the layer by Novaco and McTague¹ holds. The modulation is too small to produce any observable satellite reflections in a diffraction experiment. (b) A more strongly modulated but still truly incommensurate phase (γ phase) at

$1.19 \leq \rho \leq 1.32$, which locks into the two simplest higher-order commensurate phases possible within the framework of the special modulation (δ and ϵ phases). The γ phase can also be considered as a hexagonal heavy domain-wall phase. Simple regular arrays of domain walls can be drawn for the δ and ϵ phases. (c) A striped domain-wall phase (α phase) with superheavy walls at $1.04 \leq \rho \leq 1.16$. (d) The commensurate $(\sqrt{3} \times \sqrt{3})R 30^\circ$ phase.

ACKNOWLEDGMENTS

For a very fruitful cooperation we wish to express our warmest thanks to S. C. Fain and J. Cui, who shared their LEED results and insights with us. We also thank L. W. Bruch, T. Halpin-Healy, M. Kardar, A. D. Novaco, and O. E. Vilches for stimulating discussions and sending us manuscripts prior to publication. This work was partially funded by the German Federal Minister of Research and Technology (BMFT) under Contract Nos. 05 353 AAI2 and 05 453 AAI8.

- ¹A. D. Novaco and J. P. McTague, Phys. Rev. Lett. **38**, 1286 (1977); Phys. Rev. B **19**, 5299 (1979).
- ²M. Schick, Prog. Surf. Sci. **11**, 245 (1981); F. Y. Wu, Rev. Mod. Phys. **54**, 235 (1982); S. Ostlund and A. N. Berker, Phys. Rev. B **21**, 5410 (1980); K. Binder and D. P. Landau, in *Advances in Chemical Physics*, edited by K. P. Lawley (Wiley, New York, 1989), p. 91.
- ³For a review of the C-IC transition see, e.g., P. Bak, Rep. Prog. Phys. **45**, 587 (1982); J. Villain and M. B. Gordon, Surf. Sci. **125**, 1 (1983).
- ⁴F. C. Frank and J. H. Van der Merwe, Proc. R. Soc. **198**, 205 (1949); **198**, 216 (1949).
- ⁵P. Bak, D. Mukamel, J. Villain, and K. Wentowska, Phys. Rev. B **19**, 1610 (1979).
- ⁶J. Villain, Surf. Sci. **97**, 219 (1980).
- ⁷V. L. Pokrovsky and A. L. Talapov, Phys. Rev. Lett. **42**, 65 (1979); Zh. Eksp. Teor. Fiz. **78**, 269 (1980) [Sov. Phys.—JETP **51**, 134 (1980)].
- ⁸S. N. Coppersmith, D. S. Fisher, B. I. Halperin, P. A. Lee, and W. F. Brinkman, Phys. Rev. Lett. **46**, 549 (1981); Phys. Rev. B **25**, 349 (1982).
- ⁹M. Kardar and A. N. Berker, Phys. Rev. Lett. **48**, 1552 (1982).
- ¹⁰T. Halpin-Healy and M. Kardar, Phys. Rev. B **31**, 1664 (1985).
- ¹¹R. G. Caffisch, A. N. Berker, and M. Kardar, Phys. Rev. B **31**, 4527 (1985).
- ¹²E. D. Specht, A. Mak, C. Peters, M. Sutton, R. J. Birgeneau, K. L. D'Amico, D. E. Moncton, S. E. Nagler, and P. M. Horn, Z. Phys. B **69**, 347 (1987).
- ¹³T. Halpin-Healy and M. Kardar, Phys. Rev. B **34**, 318 (1986); T. Halpin-Healy, Ph.D. dissertation, Harvard University, 1987.
- ¹⁴K. Kern, Phys. Rev. B **35**, 8265 (1987).
- ¹⁵S. G. J. Mochrie, A. R. Kortan, R. J. Birgeneau, and P. M. Horn, Z. Phys. B **62**, 79 (1985).
- ¹⁶See, e.g., K. K. Fung, S. McKernan, J. W. Steeds, and J. A. Wilson, J. Phys. C **14**, 5417 (1981); C. H. Chen, J. M. Gibson, and R. M. Fleming, Phys. Rev. B **26**, 184 (1982).
- ¹⁷See, e.g., M. Habenschuss, C. Stassis, S. K. Sinha, H. W. Deckman, and F. H. Spedding, Phys. Rev. B **10**, 1020 (1974); P. Fischer, B. Lebech, G. Meier, B. D. Rainford, and O. Vogt, J. Phys. C **11**, 345 (1978).
- ¹⁸H. Wiechert and H. Freimuth, in *Proceedings of the 17th International Conference on Low Temperature Physics, LT-17*, edited by U. Eckern, A. Schmid, W. Weber, and H. Wühl (North-Holland, Amsterdam, 1984), p. 1015.
- ¹⁹H. Freimuth and H. Wiechert, Surf. Sci. **162**, 432 (1985).
- ²⁰F. C. Motteler, Ph.D. dissertation, University of Washington, 1986.
- ²¹H. Freimuth, Ph.D. dissertation, Johannes Gutenberg-Universität, 1989.
- ²²S. V. Hering, S. W. van Sciver, and O. E. Vilches, J. Low Temp. Phys. **25**, 793 (1976).
- ²³R. E. Ecke and J. G. Dash, Phys. Rev. B **28**, 3837 (1983).
- ²⁴H. Freimuth and H. Wiechert, Surf. Sci. **178**, 716 (1986).
- ²⁵H. Wiechert, H. Freimuth, H. P. Schildberg, and H. J. Lauter, Jpn. J. Appl. Phys. Suppl. **26**, 351 (1987).
- ²⁶M. Nielsen, J. P. McTague, and W. Ellenson, J. Phys. (Paris) Colloq. **38**, C4-10 (1977).
- ²⁷M. Nielsen, J. P. McTague, and L. Passell, in *Phase Transitions in Surface Films*, edited by J. G. Dash and J. Ruvalds (Plenum, New York, 1980), p. 127.
- ²⁸J. L. Seguin and J. Suzanne, Surf. Sci. **118**, L241 (1982).
- ²⁹F. C. Motteler and J. G. Dash, Phys. Rev. B **31**, 346 (1985).
- ³⁰F. A. B. Chaves, M. E. B. P. Cortez, R. E. Rapp, and E. Lerner, Surf. Sci. **150**, 80 (1985).
- ³¹H. Freimuth, H. Wiechert, and H. J. Lauter, Surf. Sci. **189/190**, 548 (1987).
- ³²H. P. Schildberg, H. J. Lauter, H. Freimuth, H. Wiechert, and R. Haensel, Jpn. J. Appl. Phys. Suppl. **26**, 345 (1987).
- ³³H. P. Schildberg, Ph.D. dissertation, Christian-Albrechts-Universität, 1988.
- ³⁴H. J. Lauter, H. P. Schildberg, H. Godfrin, H. Wiechert, and R. Haensel, Can. J. Phys. **65**, 1435 (1987).
- ³⁵H. J. Lauter, in *Phonons 89*, edited by S. Hunklinger, W. Ludwig, and G. Weiss (World-Scientific, Singapore, 1990), p. 871.

- ³⁶J. Cui, S. C. Fain, H. Freimuth, H. Wiechert, H. P. Schildberg, and H. J. Lauter, *Phys. Rev. Lett.* **60**, 1848 (1988); **60**, 2704 (1988).
- ³⁷J. Cui and S. C. Fain, *Phys. Rev. B* **39**, 8628 (1989); J. Cui, Ph.D. dissertation, University of Washington, 1988.
- ³⁸P. R. Kubik, W. N. Hardy, and H. Glattli, *Can. J. Phys.* **63**, 605 (1985); P. R. Kubik, Ph.D. dissertation, University of British Columbia, 1984.
- ³⁹R. E. Palmer and R. F. Willis, *Surf. Sci.* **179**, L1 (1987).
- ⁴⁰J. K. Kjems, L. Passell, H. Taub, J. G. Dash, and A. D. Novaco, *Phys. Rev. B* **13**, 1446 (1976).
- ⁴¹H. Taub, K. Carneiro, J. K. Kjems, L. Passell, and J. P. McTague, *Phys. Rev. B* **16**, 4551 (1977).
- ⁴²V. F. Sears, *Can. J. Phys.* **44**, 1279 (1966); **44**, 1299 (1966).
- ⁴³H. P. Schildberg and H. J. Lauter, *Surf. Sci.* **208**, 507 (1989).
- ⁴⁴P. W. Stephens, P. A. Heiney, R. J. Birgeneau, P. M. Horn, D. E. Moncton, and G. S. Brown, *Phys. Rev. B* **29**, 3512 (1984).
- ⁴⁵R. J. Birgeneau, H. Yoshizawa, R. A. Cowley, G. Shirane, and H. Ikeda, *Phys. Rev. B* **28**, 1433 (1983).
- ⁴⁶P. Dutta and S. K. Sinha, *Phys. Rev. Lett.* **47**, 50 (1981).
- ⁴⁷R. J. Birgeneau, P. A. Heiney, and J. P. Pelz, *Physica B* **109&110**, 1785 (1982).
- ⁴⁸V. L. P. Frank, H. J. Lauter, and P. Leiderer, *Phys. Rev. Lett.* **61**, 436 (1988).
- ⁴⁹X. Z. Ni and L. W. Bruch, *Phys. Rev. B* **33**, 4584 (1986).
- ⁵⁰A. D. Novaco, *Phys. Rev. Lett.* **60**, 2058 (1988).
- ⁵¹A. D. Novaco and J. P. Wroblewski, *Phys. Rev. B* **39**, 11 364 (1989).
- ⁵²J. M. Gottlieb and L. W. Bruch, *Phys. Rev. B* **40**, 148 (1989).
- ⁵³J. M. Gottlieb and L. W. Bruch, *Phys. Rev. B* **41**, 7195 (1990); (private communication). The mean-square displacements quoted in Refs. 52, p. 153, have to be divided by 2 to correct for a programming error.
- ⁵⁴J. E. Houston and R. L. Park, *Surf. Sci.* **21**, 209 (1970).
- ⁵⁵M. B. Gordon and F. Langon, *J. Phys. C* **18**, 3929 (1985).
- ⁵⁶C. G. Shaw, S. C. Fain, and M. D. Chinn, *Phys. Rev. Lett.* **41**, 955 (1978).
- ⁵⁷C. Tiby, H. Wiechert, and H. J. Lauter, *Surf. Sci.* **119**, 21 (1982).
- ⁵⁸H. Shiba, *J. Phys. Soc. Jpn.* **46**, 1852 (1979); **48**, 211 (1980).
- ⁵⁹A. W. Overhauser, *Phys. Rev. B* **3**, 3173 (1971).
- ⁶⁰R. Pynn, J. D. Axe, and R. Thomas, *Phys. Rev. B* **13**, 2965 (1976).
- ⁶¹J. M. Kosterlitz, *J. Phys. C* **7**, 1046 (1974).
- ⁶²D. E. Moncton, P. Heiney, R. J. Birgeneau, P. M. Horn, and S. Brown, *Phys. Rev. Lett.* **46**, 1533 (1981).
- ⁶³M. Nielsen, J. Als-Nielsen, J. Bohr, and J. P. McTague, *Phys. Rev. Lett.* **47**, 582 (1981).
- ⁶⁴J. Villain, in *Ordering in Strongly Fluctuating Condensed Matter Systems*, edited by T. Riste (Plenum, New York, 1980), p. 221.
- ⁶⁵V. L. P. Frank, H. J. Lauter, and P. Leiderer, *Jpn. J. Appl. Phys. Suppl.* **26**, 347 (1987).
- ⁶⁶H. Freimuth and H. Wiechert (unpublished).
- ⁶⁷F. F. Abraham, S. W. Koch, and W. E. Rudge, *Phys. Rev. Lett.* **49**, 1830 (1982).
- ⁶⁸F. F. Abraham and J. Q. Broughton, *Phys. Rev. Lett.* **59**, 64 (1987).
- ⁶⁹N. D. Shrimpton, B. Joos, and B. Bergersen, *Phys. Rev. B* **38**, 2124 (1988).
- ⁷⁰K. Kern, P. Zeppenfeld, R. David, and G. Comsa, *Phys. Rev. Lett.* **59**, 79 (1987).
- ⁷¹W. Weimer, K. Knorr, and H. Wiechert, *Phys. Rev. Lett.* **61**, 1623 (1988).